

EEG-EMG ANALYSIS METHOD IN HYBRID BRAIN COMPUTER INTERFACE FOR HAND REHABILITATION TRAINING

Lubo FU, Haoyang LI, Hongfei Ji*

*Department of Computer Science and Technology
School of Electronic and Information Engineering
Tongji University, Shanghai 201804, China
e-mail: {2130758, haoyangli, jhf}@tongji.edu.cn*

Jie LI*

*Translational Research Center
Shanghai YangZhi Rehabilitation Hospital
(Shanghai Sunshine Rehabilitation Center)
Tongji University
&
Department of Computer Science and Technology
School of Electronic and Information Engineering
Tongji University, Shanghai 201804, China
e-mail: nijanice@163.com*

Abstract. Brain-computer interfaces (BCIs) have demonstrated immense potential in aiding stroke patients during their physical rehabilitation journey. By reshaping the neural circuits connecting the patient's brain and limbs, these interfaces contribute to the restoration of motor functions, ultimately leading to a significant improvement in the patient's overall quality of life. However, the current BCI primarily relies on Electroencephalogram (EEG) motor imagery (MI), which has relatively coarse recognition granularity and struggles to accurately recognize specific hand movements. To address this limitation, this paper proposes a hybrid BCI framework based on Electroencephalogram and Electromyography (EEG-

* Corresponding author

EMG). The framework utilizes a combination of techniques: decoding EEG by using Graph Convolutional LSTM Networks (GCN-LSTM) to recognize the subject's motion intention, and decoding EMG by using a convolutional neural network (CNN) to accurately identify hand movements. In EEG decoding, the correlation between channels is calculated using Standardized Permutation Mutual Information (SPMI), and the decoding process is further explained by analyzing the correlation matrix. In EMG decoding, experiments are conducted on two task paradigms, both achieving promising results. The proposed framework is validated using the publicly available WAL-EEG-GAL (Wearable interfaces for hand function recovery Electroencephalography Grasp-And-Lift) dataset, where the average classification accuracies of EEG and EMG are 0.892 and 0.954, respectively. This research aims to establish an efficient and user-friendly EEG-EMG hybrid BCI, thereby facilitating the hand rehabilitation training of stroke patients.

Keywords: Hybrid BCI, EEG, EMG, GCN, neural networks

1 INTRODUCTION

Stroke is a debilitating condition caused by the blockage or rupture of blood vessels, resulting in damage to brain cells. It often leads to various neurological deficits, including unilateral paralysis, cognitive impairment, and language difficulties. Among the challenges faced by stroke survivors, upper limb impairment significantly impacts their ability to perform essential activities of daily living (ADLs) such as eating, dressing, and personal hygiene. Given the intricate and precise movements required for these tasks, effective hand rehabilitation is crucial to restore patients' independence in performing these fundamental activities [1, 2].

1.1 Rehabilitation Training Based on EEG MI

Motor imagery (MI) refers to the mental process of envisioning movement without actually physically executing it [3, 4, 5, 6, 7]. It has been widely utilized by both healthy individuals for learning new movement skills during exercise [8] and stroke patients during rehabilitation training [9]. The underlying principle behind MI lies in the activation of brain regions within the sensorimotor network [10]. Thus, for patients facing difficulties in performing physical movements during rehabilitation, MI can be employed to activate partially damaged motor networks, aiding them in the gradual restoration of movement [11]. Numerous studies have demonstrated the effectiveness of EEG-based MI in rehabilitation.

EEG recordings are obtained by measuring the potential between a signal electrode and a reference electrode placed on the scalp, which is easily contaminated by eye and muscle movement. Furthermore, EEG exhibits limitations in spatial resolution, typically ranging from 5 to 9 centimeters [12], and it can only capture

neuronal population potentials in broad brain regions. As a result, EEG is primarily capable of detecting coarse-grained changes in brain signals, often unable to discern the finer and more intricate movements associated with the affected limb. Thus, relying solely on EEG poses challenges in perceiving and capturing the complexities of movement.

1.2 Dynamic Graph Convolutional Networks for BCIs

Traditionally, EEG decoding has involved processing data from each channel independently, without considering the inter-channel correlations. However, by treating EEG as graph-structured data, it becomes possible to leverage the relationships between channels and achieve more comprehensive EEG decoding. One approach to handling graph-structured data is to use the graph convolutional networks (GCN) [13]. Notably, Song et al. successfully applied GCN to EEG emotion recognition in 2018, yielding promising outcomes [14].

To address the challenge of limited EEG data volume, Zhang et al. proposed GCB-net [15]. GCB-net utilizes graph convolution layers to explore the correlations between EEG channels and employs the broad learning system (BLS) mechanism to map the extracted features into a wider feature space, resulting in enhanced robustness. Moreover, to further uncover the relationships between EEG channels, dynamic graph convolution has gained significant traction [16]. Dynamic graph neural networks employ a learnable adjacency matrix as a parameter, which is updated during the training process [17, 18, 19].

In this study, a similar approach is adopted, where graph convolution is employed to capture the correlations between EEG channels. Additionally, LSTM is utilized to address the temporal dynamics inherent in EEG signals.

1.3 EEG-EMG-Based Hybrid BCIs

EMG, obtained by recording the electrical activity of skeletal muscles through surface sensors, possesses notable advantages over EEG. It exhibits good stability, high signal strength, and the ability to discern finer body movements in healthy individuals. Many studies [20, 21, 22, 13, 23] have demonstrated that EMG-based techniques can achieve high accuracy in multi-gesture recognition with fewer leads and shorter calibration times.

Research on the EEG-EMG-based Hybrid BCIs has already been initiated. Leeb et al. [24] conducted a fusion study using EEG and EMG signals to enhance the classification accuracy of MI. Lin et al. [25] combined visually evoked potentials (SSVEP) with EMG to increase the number of targets and improve information transmission rates. Sarasola-Sanz et al. [26] employed EEG and EMG to control a mechanical exoskeleton, enabling control of a seven-degree-of-freedom robotic arm. Some studies have explored the coupling of EEG and EMG signals. Tun et al. [27, 28] investigated the functional coupling between EEG and EMG during four distinct movements. Soundirarajan et al. [29] evaluated the coupled responses

of facial muscles and the brain to various motor visual stimuli by analyzing the information embedded in EEG and EMG signals.

In this study, the participants' active intentions are captured through EEG, utilizing EEG decoding to monitor their motor intentions. Additionally, leveraging the fine-grained classification capability of EMG, action recognition is achieved through EMG decoding.

2 MODEL FRAMEWORK

This section introduces the comprehensive framework employed in this study, depicted in Figure 1. The framework utilizes both EEG and EMG signals for hand rehabilitation training. Firstly, the EEG signals are decoded to detect the user's intended movements. Subsequently, the decoded intention is used to guide the decoding of the EMG signals, facilitating the classification of specific hand actions. External devices are employed to provide additional support for the rehabilitation training process.

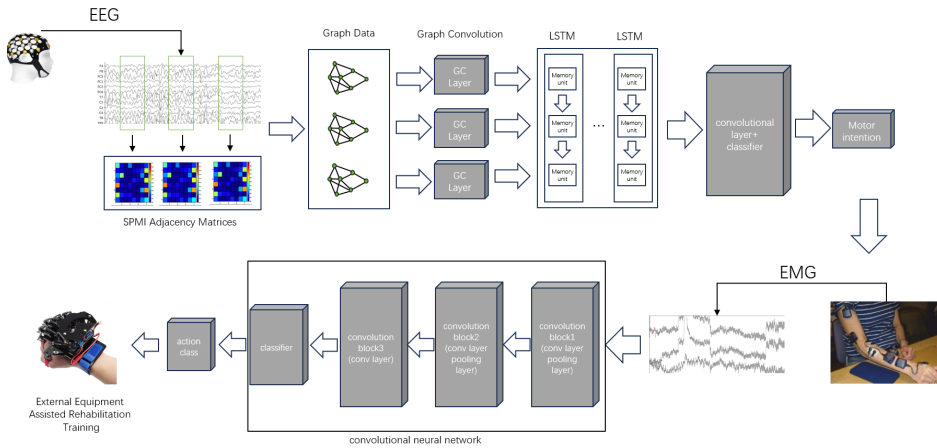


Figure 1. Overall framework: After the EEG signal is obtained through the device, it is processed into serialized graph structure data, and then processed by GCN-LSTM to detect motion intention. Then, for the obtained EMG, we use CNN to decode and realize action recognition, so as to help the subjects to carry out hand rehabilitation training.

We commence by acquiring 32-channel EEG data through the utilization of an EEG cap. Subsequently, the EEG data are segmented into four segments. For each segment, the pairwise SPMI between each channel is calculated, resulting in the construction of a relational adjacency matrix. This matrix facilitates the creation of a serialized graph structure representation of the EEG data.

Next, the decoding process begins by employing a graph convolutional (GC) layer for each segment. Additionally, for each vertex, all its corresponding segments

form a sequence, which is then processed using a Long Short-Term Memory (LSTM) network. To enable deeper decoding, a convolutional block is applied, followed by a classification layer that generates predictions regarding the user's motion intentions.

Simultaneously, the EMG data is processed using a CNN composed of three convolutional blocks. The EMG decoding primarily focuses on extracting relevant information from the temporal dimension.

3 MATERIALS AND METHODS

3.1 Data Description

We utilize the publicly available WAL-EEG-GAL dataset [30] for our study. This dataset captures simultaneous EEG and EMG recordings from 12 subjects while they perform repetitive grasping and lifting trials. Each subject participates in several series, and each series consists of 34 repeated trials.

During each trial, the participants are instructed to reach out and grasp a small object using their thumb and forefinger, lift it into the air, hold it for a few seconds, and then lower it back to its initial position. The entire process lasts approximately 8 seconds, with LED indicators used to signal the lifting and lowering phases, while other aspects of the rhythm are controlled by the participants themselves. A total of 32 electrodes are used to record the EEG signals, while 5 electrodes are employed for EMG recordings. The EEG signals are sampled at a frequency of 500 Hz, and the EMG signals are sampled at 4000 Hz.

Across different series, the weight of the grasped object (150 g, 300 g, 600 g) and the surface material (sandpaper, suede, silk) varied. However, for our study, we focus solely on the series with object weight variations, while ensuring that the surface material remained consistent (sandpaper).

As shown in Figure 2, the upper two figures respectively represent the schematic diagram of the EEG channel and the schematic diagram of the EMG channel. Among them, for EEG, we adopt the international standard 10-20 system, and use 1-32 channels as shown in the figure. For EMG, we use 5 positions on the arm: the anterior deltoid (AD), brachioradial (BR), flexor digitorum (FD), common extensor digitorum (CED), and the first dorsal interosseus muscles (FDI). The scale below indicates the key time points in a trial process, and a trial lasts 8 s. Based on the actions performed at each time point and whether the object is touched, the trial can be divided into two distinct stages. The first stage, lasting from 0 to 4 seconds, represents the initial stage of movement. The subsequent stage, spanning from 4 to 8 seconds, corresponds to the specific execution stage of the movement. More specifically, the period from 0 to 2 seconds represents the resting stage, while the interval from 2 to 4 seconds corresponds to the action stage. The EEG signals recorded during these two stages can be analyzed to enable the model to recognize the intended movement.

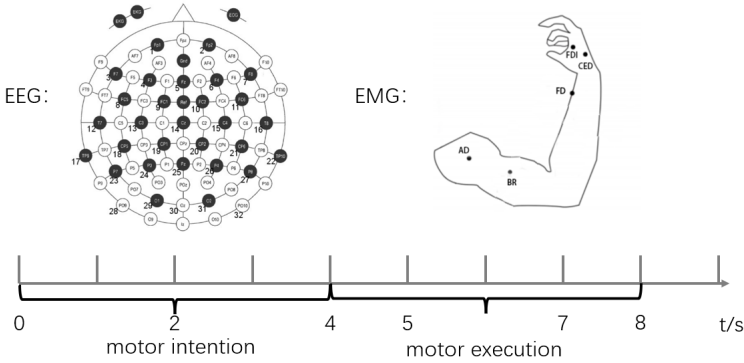


Figure 2. An introduction to each time point of a trial, 2 s: the LED light is on, indicating that the subject starts to move; 2–4 s: the subject reaches for the object; 4–5 s: the object leaves the table; 8 s: the object is put back on the table. We use 0–4 s EEG data to detect motion intention, and 4–8 s EMG data to classify motion execution.

3.2 Data Processing

3.2.1 EEG Processing

The original EEG data is represented as $X \in \mathbb{R}^{c \times t}$, where c denotes the number of channels ($c = 32$), and t represents the number of sampling points ($t = 4000 = 8 \times 500$). In this study, the EEG data of the first 4 s is used for the detection of motion intention. Specifically, the data from 0 to 2 seconds is assigned as class 0, while the data from 2 to 4 seconds is assigned as class 1. Consequently, the value of t is reduced to 1000 (2×500). To streamline the computational load, we downsample the EEG data by reducing its frequency to half of the original. Additionally, to eliminate noise and extract signals relevant to motion classification, a band-pass filter with a range of 4 to 35 Hz is applied to the EEG data.

EEG data represents a time-series signal. To fully leverage its temporal characteristics, the EEG signal of a trial is partitioned into T segments (in this study, T is set to 4), resulting in a data representation of $(X_i)_{i \in \mathbb{Z}_T}$, where $\mathbb{Z}_T := \{1, 2, \dots, T\}$. Additionally, EEG comprises multiple channels of data, and there exists a certain interrelation between these channels. By treating EEG as graph-structured data, we can explore the relationships between channels and comprehensively analyze the EEG signal.

For each step i , each channel of EEG is treated as a vertex v_i . By calculating SPMI, we derive the connections e_i between channels, leading to the generation of an adjacency matrix A_i . Consequently, undirected graphs $G_i = (V_i, E_i)$ are formed. The data corresponding to each channel serves as the feature vector for the respective vertex X_i .

3.2.2 EMG Processing

The original EMG data is represented as $Y \in \mathbb{R}^{c \times t}$, where c denotes the number of channels ($c = 5$), and t represents the number of sampling points ($t = 32\,000 = 8 \times 4\,000$). In this study, the EMG data from the last 4 seconds is utilized for classification, resulting in t being equal to 16 000 ($4 \times 4\,000$).

To begin with, the EMG signal is downsampled from 4 000 Hz to 250 Hz in order to reduce the sampling frequency. Subsequently, a filtering process is applied to the signal within the frequency range of 0 Hz to 100 Hz to remove unwanted frequencies and retain the relevant information for further analysis.

3.3 Classification Methods

In this section, two primary models are introduced for processing EEG and EMG signals, respectively. The GCN-LSTM is utilized to handle the EEG data, while the CNN is employed to process the EMG data.

3.3.1 EEG Classification Based on GCN-LSTM

We use a GCN-LSTM to process EEG, which consists of the following two components:

- GCN: Graph convolution is capable of handling graph-structured data, allowing for the processing of feature information for each vertex while considering the connections between vertices. However, it does not possess the ability to handle time series information.
- LSTM: LSTM facilitates the backward propagation of time series information through its memory unit, making it advantageous for handling time series data. However, it may not effectively utilize the connection relationships between vertices in graph-structured data.

We leverage the strengths of both GCN and LSTM to construct a GCN-LSTM for EEG processing, as shown in Figure 3.

For EEG, we preprocess it into serialized graph structured data. Here, each channel of the EEG is represented as a vertex on the graph, and the relationship between the vectors and among the channels constitutes the adjacency matrix of the graph. Let $(G_i)_{i \in \mathbb{Z}_T}$ with $\mathbb{Z}_T := \{1, 2, \dots, T\}$ represent a finite sequence of undirected graphs $G_i = (V_i, E_i)$, where $V_i \in V \forall i \in \mathbb{Z}_T$. All graphs in the sequence share the same set of vertices, but the vertex feature vectors and adjacency matrices may differ among the graphs.

In this study, SPMI [31] is used to calculate the connection between vertices, so as to obtain the adjacency matrix A_i . For two channel vectors X and Y of a signal, their correlation can be calculated as follows.

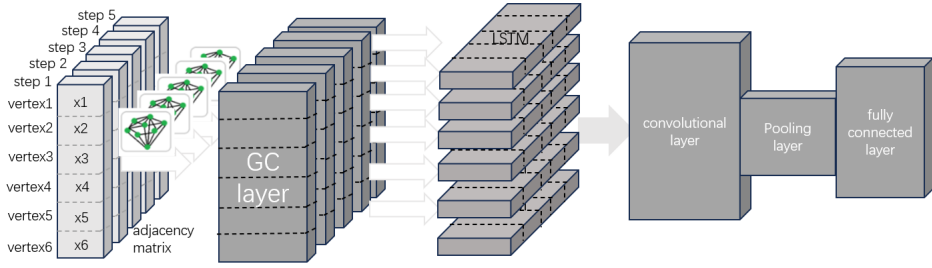


Figure 3. GCN-LSTM: A model for classifying serialized graph-structured EEG, consisting of GC layers, LSTM layers, and convolutional blocks

First, calculate the permutation entropy of the vector X , as follows:

$$PE_X = - \sum_{i=1}^{n!} P_X(i) \log(P_X(i)), \tag{1}$$

where $P_X(i)$ is the empirical probability of the i^{th} ordered pattern of X , and n is the dimension of X . Then the joint PE of signals X and Y is defined as follows:

$$PE_{X,Y} = - \sum_{i=1}^{n!} \sum_{j=1}^{n!} P_{X,Y}(i, j) \log(P_{X,Y}(i, j)), \tag{2}$$

where $P_{X,Y}(i, j)$ is the joint probability of permutation of X and Y . Finally the $SMPI$ of X and Y can be calculated as follows:

$$SMPI_{X,Y} = \frac{PE_X + PE_Y - PE_{X,Y}}{PE_{X,Y}}. \tag{3}$$

As depicted in the figure, the serialized graph-structured EEG data can be segmented into T steps. To decode each step, we utilize a GC layer, and a total of T parallel GC layers are employed to process all T steps. Specifically, at step i , the vertex feature vector set $X_i^0 \in \mathbb{R}^{|V| \times d}$ serves as the input to the GCN layer. The adjacency matrix A_i of the graph is employed to aggregate the neighborhood information. Subsequently, a weight matrix $W_i \in \mathbb{R}^{d \times d}$ is applied to update the vertex embedding vector set. The mathematical form of this process can be expressed as follows:

$$\begin{aligned} X_i^1 &= GCL_i(A_i, X_i^0, W_i), \\ &:= \sigma(A_i X_i^0 W_i), \end{aligned} \tag{4}$$

where $X_i^1 \in \mathbb{R}^{c \times d}$, σ is an activation function.

For vertex j , its T steps form a sequence, expressed as $(x_{i,j})_{i \in \{1,2,\dots,T\}}$. These sequences are then processed by an LSTM layer, with a total of c such layers used to

process all \mathbf{c} vertices. For a given vertex \mathbf{j} , the output of the LSTM layer is obtained through the following calculation steps.

The first step involves determining which information should be retained or forgotten from the cell state. This decision is governed by the “forget gate” layer, which uses a sigmoid function to determine whether to completely forget or partially retain information from the previous time step. At step i , the calculation can be expressed as follows:

$$f_{i,j} = \sigma(W_f \cdot [h_{i-1,j}, x_{i,j}] + b_f). \tag{5}$$

The second step involves generating new information that we need to incorporate for updating. This step comprises two parts. The first part is an “input gate” layer that utilizes the sigmoid function to determine the values that should be updated. The second part involves a tanh layer that generates new candidate values and combines them together to yield the candidate values. The process can be described as follows:

$$C_{i,j} = f_{i,j} * C_{i-1,j} + m_i * \tilde{C}_{i-1,j}. \tag{6}$$

The final step is to determine the output of the model. Initially, an initial output is obtained through the sigmoid layer. This output is then scaled to a range of -1 to 1 using the tanh function. The scaled output is multiplied element-wise with the output obtained from the sigmoid layer to obtain the final output of the model.

$$o_{i,j} = \sigma(W_o[h_{i-1,j}, x_{i,j}] + b_o), \tag{7}$$

$$h_{i,j} = o_{i,j} * \tanh(C_{i,j}). \tag{8}$$

We obtain the hidden state of the last step as the output of the LSTM, so we have

$$x_j^2 = LSTM(x_j^1). \tag{9}$$

Here, the symbol σ represents the sigmoid function, as illustrated in Equation (9), and \tanh denotes the hyperbolic tangent function, as depicted in Equation (10):

$$\sigma(x) = \frac{1}{1 + e^{-x}}, \tag{10}$$

$$\tanh(x) = \frac{e^x - e^{-x}}{e^x + e^{-x}}. \tag{11}$$

The corresponding sequence $(x_{i,j})_{i \in \{1,2,\dots,T\}}$ is transformed into a sequence $x_j^1 \in \mathbb{R}^{d^1}$ representing the embedded feature vector for vertex \mathbf{j} . In turn, all \mathbf{c} embedded feature vectors are concatenated into a vertex vector set $X^2 \in \mathbb{R}^{c \times d^2}$. A convolution block is then applied to further decode these features, followed by a fully connected layer and a softmax function for obtaining the final classification probabilities.

$$y = \text{softmax}(\text{linear}(\sigma(\text{Covn}(X^2))). \tag{12}$$

By analyzing the classification results, we can get the results of motion intention detection.

3.3.2 CNN-Based EMG Classification

We propose a novel approach for efficiently decoding EMG signals using a CNN, as illustrated in Figure 4. After collecting EMG on the arm using 5 EMG electrodes, some preprocessing operations are performed on the raw data. We reduce the data dimension by downsampling, remove noise and impurities by filtering, and obtain useful signals. The processed data is then decoded using a CNN. Considering the limited number of EMG channels ($c = 5$), we mainly apply convolutions over the time dimension. The architecture comprises three convolutional blocks, where the first two are composed of a single convolutional layer followed by a max-pooling layer, while the third block utilizes only convolutional layers. The ReLU activation function is utilized throughout the network, and dropout is employed after each convolutional layer to alleviate overfitting. For each convolutional block i , the input is Y^i , which is then processed as follows.

$$Y^{i+1} = \text{MaxPooling}(\text{Conv2D}(Y^i)). \quad (13)$$

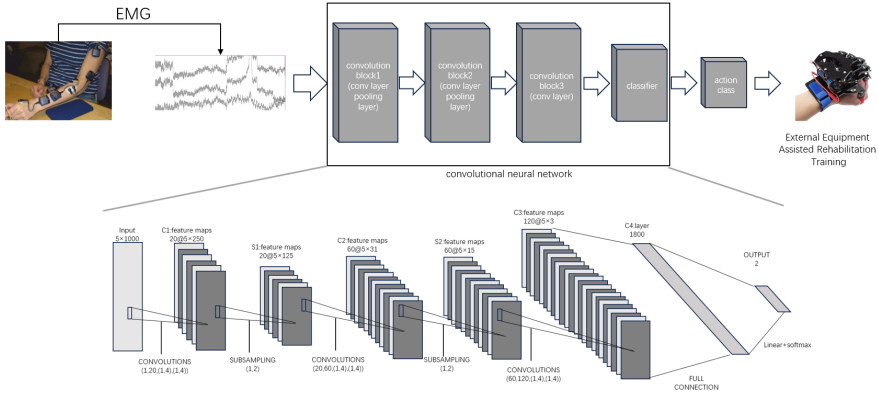


Figure 4. CNN: A convolutional network for EMG classification, consisting of three convolutional blocks, which mainly decodes from the temporal dimension of EMG

Following convolutional blocks, we employ a fully connected layer to further process the extracted features, and subsequently apply a linear layer and softmax function to obtain the classification probability. Specifically, the linear layer computes the weighted sum of the features, and then the softmax function maps the resulting vector to a probability distribution over the classes. This allows for accurate classification of EMG signals with a high degree of confidence.

$$y = \text{Softmax}(\text{Linear}(\text{Flatten}(Y))). \quad (14)$$

After obtaining the classification results of EMG, control signals are sent to the peripheral devices (such as mechanical gloves) connected to the computer to assist

the subject's movement, thereby helping the subject to perform hand rehabilitation training.

4 RESULTS AND DISCUSSION

4.1 Intention Detection

4.1.1 Experiments Settings

We employ the GCN-LSTM model to process the serialized graph structure of EEG signals and detect movement intention. The training of the model consists of 200 epochs with a batch size of 10. To optimize the model, we use the Adam optimizer with a learning rate of $1e-3$ and a weight decay parameter of $1e-3$. The loss function is implemented as the sum of cross-entropy between the predicted label and the true label. L2 regularization is also applied during the training phase to reduce overfitting. During the evaluation phase, the average accuracy of test data serves as the key metric to assess performance of the model. Our evaluation results demonstrate the effectiveness of the proposed GCN-LSTM approach in accurately decoding EEG signals for estimating movement intention.

The model is evaluated in two ways. On the one hand, the correlation between channels is calculated, and the interpretability is illustrated by analyzing the connection of channels. On the other hand, the validity of the model is verified by the average accuracy rate.

4.1.2 Experiments Results

Our proposed model is evaluated for its accuracy in detecting EEG motion intentions. We conduct experiments with 12 subjects and compared the results with the CSP + SVM model [32] as the baseline. As shown in Figure 5, the experimental results demonstrate that our model outperforms the baseline model across all subjects. Specifically, the accuracy rate for subjects 1, 2, 4, 7, 9, 10, and 11 exceeded 90%, while the performance for test 5 is suboptimal, achieving only slightly above 70%. This lower accuracy for test 5 may be attributable to poorer signal quality in that particular experiment.

To further validate the interpretability of our model, we will conduct experiments to analyze its performance. In each trial (0–8s), we will divide the data into four segments, each consisting of 2 seconds. For each segment, we will calculate the inter-channel correlation using SPMI. Interpretability of our model will be validated through experiments.

Figure 6 shows the channel correlation matrix of the four stages and the corresponding connection visualization. The matrix is represented by 6 a), 6 b), 6 e), and 6 f) corresponding to each stage. The figure is structured horizontally from left to right and vertically from top to bottom. The channel order follows the same sequence as that of channels (1–32) shown on the 10-20 system in Figure 2.

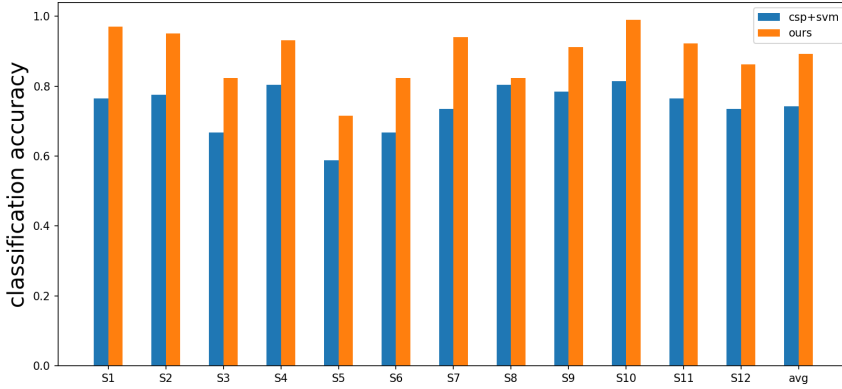
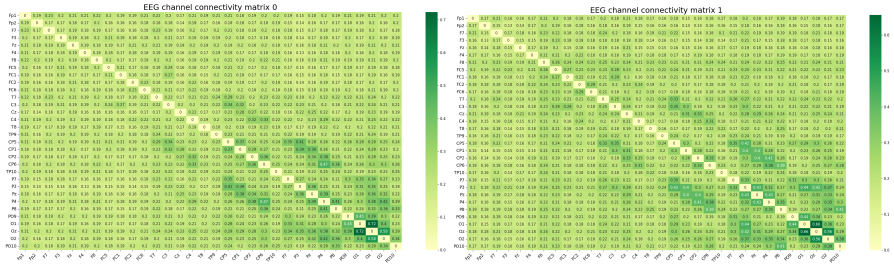


Figure 5. EEG classification accuracy

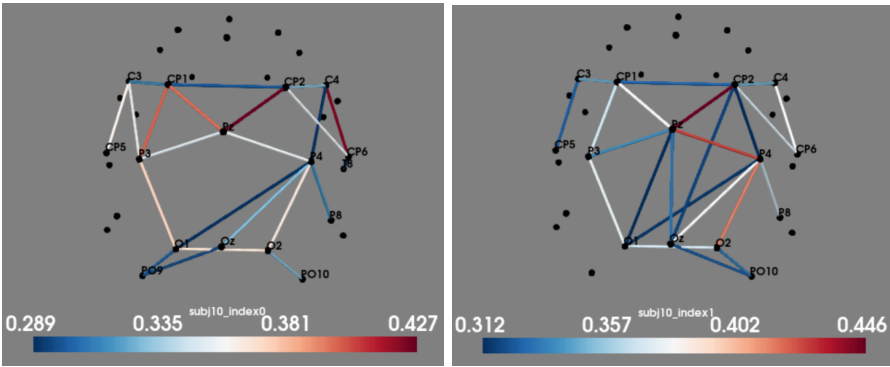
The number bar on the right side of each figure shows the strength of the relationship between channels. The relationship becomes stronger from bottom to top. Figures 6 c), 6 d), 6 g), and 6 h) are the corresponding connection visualization diagrams. During the creation process, the 20 connections with the highest connection strength are selected, and the connections between the channels with a distance of less than 5 cm are removed to reduce the interference caused by the close distance.

Figure 6 reveals two notable patterns. First, although the overall data corresponds to 32 channels, only about 15 channels exhibit significant connectivity during the motion process. Second, the areas with strong connectivity are motor and visual areas, which are consistent with the form of the task action. Although the connection between the leads changes in the four stages, the channels with strong connectivity remain the same. This indicates that the subject's motor and visual areas remained active throughout this period. To enhance the universality of the channel selection process, we employ a method to refine it further. Initially, we select a representative sample consisting of 12 subjects to undergo the channel selection process. Each subject goes through four distinct stages, thereby generating a total of 48 data pieces. Subsequently, we compute the channel correlation matrix using these data samples. From each correlation matrix, we identify the 15 connections with the highest correlation values. We take out the channels associated with these connections and proceed by tallying the frequency of occurrence for each channel across the 48 sets of data. This frequency count enables us to determine the popularity of each channel within the dataset. Ultimately, to facilitate our experimentation, we select the top 15 channels ('P3', 'P4', 'Pz', 'Oz', 'O2', 'CP1', 'O1', 'CP2', 'CP5', 'CP6', 'P8', 'PO9', 'P7', 'PO10', 'C3') with the highest frequency of occurrence. These channels will be utilized for further analysis and investigation. This suggests that these channels are the most informative.



a) 0-2s

b) 2-4s



c) 0-2s

d) 2-4s

To demonstrate that the well-connected channels provide more effective information, we conduct a series of controlled experiments. Specifically, we limit the data used for motion intent recognition to the 15 channels exhibiting strong connectivity. The results are shown in the Figure 7.

As displayed in Figure 7, despite using data from less than half of the original channels, the accuracy rate did not decrease significantly. Notably, Tests 4 and 11 even achieved results that are equal to or greater than the original 32-channel setup. In terms of average accuracy, the 15-channel configuration is only 0.07 lower than the 32-channel configuration. These findings demonstrate that effective channels can be identified through analyzing channel connectivity. This not only provides an explanation for EEG decoding, but also facilitates the development of portable EEG devices.

4.2 Action Classification

4.2.1 Experiments Settings

In this study, an action classification model based on CNN is trained and evaluated using EMG data. The model is trained using 500 epochs and a batch size of 10, with

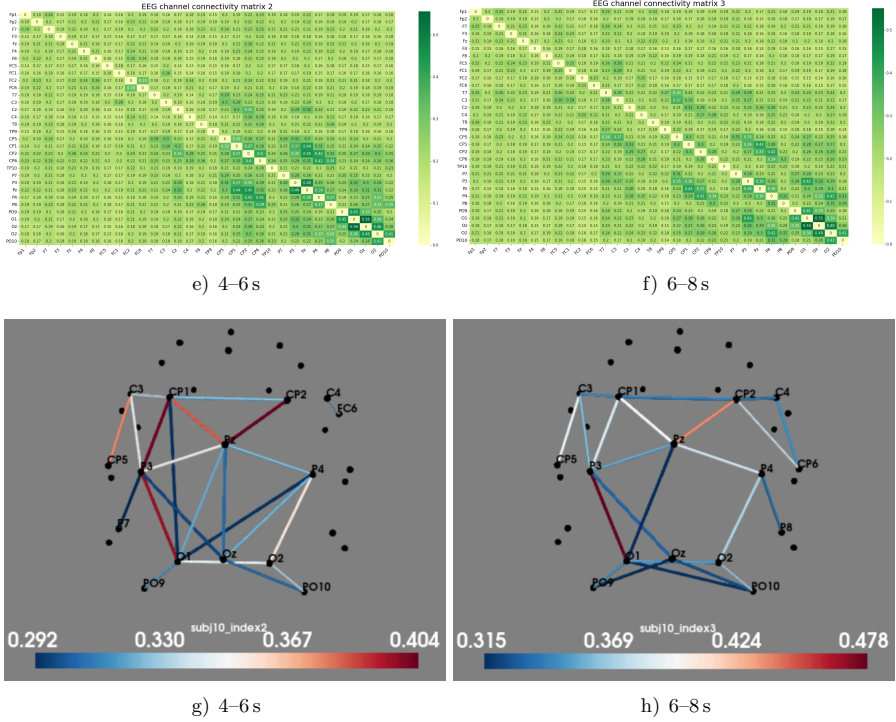


Figure 6. The 4-stage channel connectivity matrix and its corresponding connection diagram (a and c, b and d, e and g, f and h)

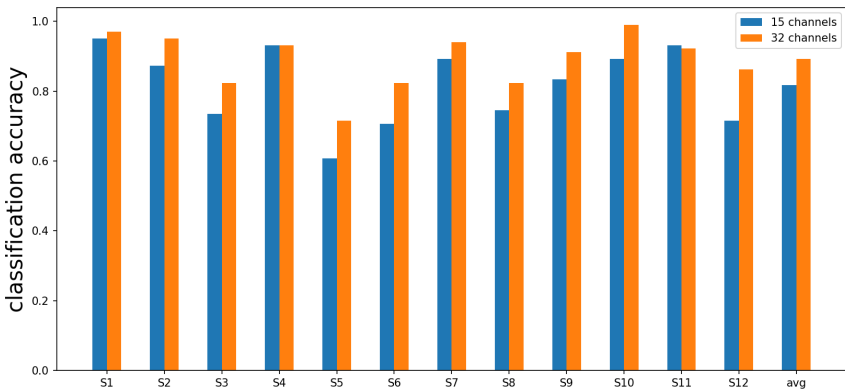


Figure 7. The accuracy rate: 15 channels vs 32 channels

the Adam optimizer and a learning rate of $1e-3$. The loss function is defined as the sum of cross entropy between the predicted and actual labels. During evaluation, average accuracy of the test data is used as a metric to assess performance of the model.

4.2.2 Experiments Results

The present study aimed to decode EMG signals for the purpose of identifying different weights of lifted objects (i.e., 150 g, 300 g, 600 g). Effectiveness of the proposed model is evaluated using classification accuracy for these three types of data. Additionally, the proposed model is compared to a benchmark model, lightgbm [33], with the results shown in Figure 8.

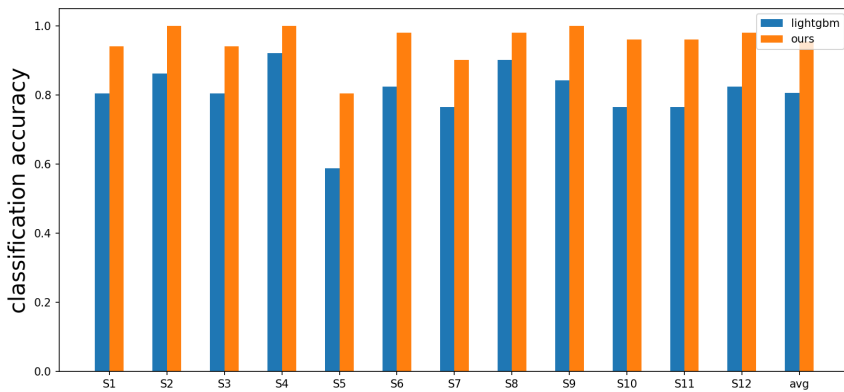


Figure 8. EMG: Classification accuracy for lifting different weights

Figure 8 illustrates the classification accuracy results for the proposed model, which are found to be excellent, with the exception of subject 5, for whom the accuracy is lower than 0.9. This may be attributable to poor signal quality from that subject. Furthermore, compared to the baseline model lightgbm, the proposed model demonstrated better performance across all tests. Specifically, the average accuracy of the proposed model (0.954) is about 0.15 higher than that of the baseline model (0.806), indicating its effectiveness.

To examine the generality of our model, we conduct additional experiments on different task formats. In a given trial (0–8 s), subjects performed a series of actions, including reaching out (2–4 s), lifting the object (4–6 s), and putting it down (6–8 s). By identifying these three actions, our model not only demonstrates its versatility but also provides opportunities for rehabilitation training. As shown in Figure 9, we compare the accuracy of the proposed model to that of the benchmark model, lightgbm. Overall, the classification accuracy of the proposed model is excellent, achieving an average accuracy of 0.937, which is 0.04 higher than that of the

benchmark model (0.897). These results further underscore the effectiveness and generality of our proposed model.

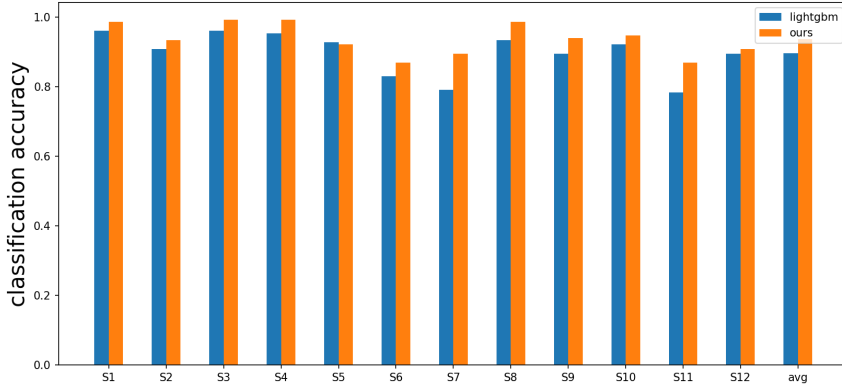


Figure 9. EMG: Classification accuracy of different actions

5 CONCLUSION AND FUTURE WORK

This study proposes a novel framework for hand rehabilitation training using EEG and EMG signals. EEG is used to detect movement intention, while EMG is utilized to recognize specific hand gestures. To decode EEG signals, we employ GCN-LSTM, which achieved an average classification accuracy of 0.892 surpassing the benchmark classifier (0.742) and demonstrating the effectiveness of our model. Additionally, we analyze channel connectivity to explain the interpretability of the model, finding that using a subset of highly connected channels (15 channels) resulted in only a 0.07 decrease in accuracy when the amount of data is halved, which indicates the potential for simplifying the number of EEG channels needed. Using a CNN, EMG signals are decoded to recognize different hand movements in two different tasks, with the proposed model achieving an average accuracy of 0.954 and 0.937, respectively, which outperformed the benchmark model lightgbm. These results highlight the effectiveness and generalizability of our proposed model for hand rehabilitation training. We can apply the framework proposed in this study to the hybrid BCI system, combined with the hardware equipment of the BCI, so as to realize the patient's hand rehabilitation training. Specifically, the user's movement intention is identified through EEG decoding, and EMG decoding is used to realize specific hand movements or fine power control, and then external devices such as mechanical gloves are used to assist the subject's movement, and the system gives the subject certain feedback. Through this series of processes, the patient's neural circuit is rebuilt to achieve rehabilitation training. In addition, future work in this area should focus on the following aspects:

- In the aspect of motion intention recognition based on EEG, by improving the model, effective monitoring can be carried out while reducing the number of data sampling points, thereby reducing the response time of the BCI system and improving usability.
- Further analyzing channel connectivity in EEG to improve interpretability and identify channels that are closely related to different actions. This can help select appropriate channels for specific tasks, thereby aiding in the development of portable BCI devices.
- Furthermore, the connectivity between EEG and EMG can be explored to discuss the mechanisms behind the operation of hybrid BCI systems.

6 FUNDING

This work is supported by the Shanghai Municipal Science and Technology Major Project (2021SHZDZX0100) and the Fundamental Research Funds for the Central Universities, and the Science and Technology Innovation Action Plan of the Shanghai Science and Technology Commission (19441908000).

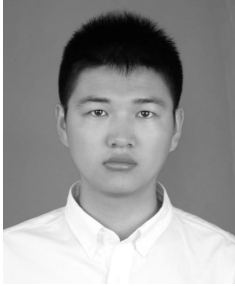
REFERENCES

- [1] YUE, Z.—ZHANG, X.—WANG, J.: Hand Rehabilitation Robotics on Poststroke Motor Recovery. *Behavioural Neurology*, Vol. 2017, 2017, Art.No. 3908135, doi: 10.1155/2017/3908135.
- [2] NICHOLS-LARSEN, D. S.—CLARK, P. C.—ZERINGUE, A.—GREENSPAN, A.—BLANTON, S.: Factors Influencing Stroke Survivors' Quality of Life During Subacute Recovery. *Stroke*, Vol. 36, 2005, No. 7, pp. 1480–1484, doi: 10.1161/01.STR.0000170706.13595.4f.
- [3] JEANNEROD, M.: Mental Imagery in the Motor Context. *Neuropsychologia*, Vol. 33, 1995, No. 11, pp. 1419–1432, doi: 10.1016/0028-3932(95)00073-C.
- [4] MÜLLER-PUTZ, G. R.—SCHERER, R.—PFURTSCHELLER, G.—RUPP, R.: EEG-Based Neuroprosthesis Control: A Step Towards Clinical Practice. *Neuroscience Letters*, Vol. 382, 2005, No. 1-2, pp. 169–174, doi: 10.1016/j.neulet.2005.03.021.
- [5] ZHAO, Q. B.—ZHANG, L. Q.—CICHOCKI, A.: EEG-Based Asynchronous BCI Control of a Car in 3D Virtual Reality Environments. *Chinese Science Bulletin*, Vol. 54, 2009, No. 1, pp. 78–87, doi: 10.1007/s11434-008-0547-3.
- [6] MENG, J.—ZHANG, S.—BEKYO, A.—OLSOE, J.—BAXTER, B.—HE, B.: Noninvasive Electroencephalogram Based Control of a Robotic Arm for Reach and Grasp Tasks. *Scientific Reports*, Vol. 6, 2016, No. 1, Art.No. 38565, doi: 10.1038/srep38565.
- [7] FOONG, R.—ANG, K. K.—QUEK, C.—GUAN, C.—PHUA, K. S.—KUAH, C. W. K.—DESHMUKH, V. A.—YAM, L. H. L.—RAJESWARAN, D. K.—TANG, N.—CHEW, E.—CHUA, K. S. G.: Assessment of the Efficacy of EEG-Based MI-BCI with Visual Feedback and EEG Correlates of Mental Fatigue for Upper-Limb

- Stroke Rehabilitation. *IEEE Transactions on Biomedical Engineering*, Vol. 67, 2020, No. 3, pp. 786–795, doi: 10.1109/TBME.2019.2921198.
- [8] MURPHY, S. M.: Imagery Interventions in Sport. *Medicine and Science in Sports and Exercise*, Vol. 26, 1994, No. 4, pp. 486–494, doi: 10.1249/00005768-199404000-00014.
- [9] SHARMA, N.—POMEROY, V. M.—BARON, J. C.: Motor Imagery: A Backdoor to the Motor System After Stroke? *Stroke*, Vol. 37, 2006, No. 7, pp. 1941–1952, doi: 10.1161/01.STR.0000226902.43357.fc.
- [10] KRAEUTNER, S.—GIONFRIDDO, A.—BARDOUILLE, T.—BOE, S.: Motor Imagery-Based Brain Activity Parallels That of Motor Execution: Evidence from Magnetic Source Imaging of Cortical Oscillations. *Brain Research*, Vol. 1588, 2014, pp. 81–91, doi: 10.1016/j.brainres.2014.09.001.
- [11] JOHNSON, S. H.: Imagining the Impossible: Intact Motor Representations in Hemiplegics. *NeuroReport*, Vol. 11, 2000, No. 4, pp. 729–732, doi: 10.1097/00001756-200003200-00015.
- [12] BABILONI, C.—PIZZELLA, V.—DEL GRATTA, C.—FERRETTI, A.—ROMANI, G. L.: Chapter 5. Fundamentals of Electroencefalography, Magnetoencefalography, and Functional Magnetic Resonance Imaging. *International Review of Neurobiology*, Vol. 86, 2009, pp. 67–80, doi: 10.1016/s0074-7742(09)86005-4.
- [13] KIPF, T. N.—WELLING, M.: Semi-Supervised Classification with Graph Convolutional Networks. *CoRR*, 2016, doi: 10.48550/arXiv.1609.02907.
- [14] SONG, T.—ZHENG, W.—SONG, P.—CUI, Z.: EEG Emotion Recognition Using Dynamical Graph Convolutional Neural Networks. *IEEE Transactions on Affective Computing*, Vol. 11, 2020, No. 3, pp. 532–541, doi: 10.1109/TAFFC.2018.2817622.
- [15] ZHANG, T.—WANG, X.—XU, X.—CHEN, C. L. P.: GCB-Net: Graph Convolutional Broad Network and Its Application in Emotion Recognition. *IEEE Transactions on Affective Computing*, Vol. 13, 2019, No. 1, pp. 379–388, doi: 10.1109/TAFFC.2019.2937768.
- [16] MANESSI, F.—ROZZA, A.—MANZO, M.: Dynamic Graph Convolutional Networks. *Pattern Recognition*, Vol. 97, 2020, Art.No. 107000, doi: 10.1016/j.patcog.2019.107000.
- [17] SUN, M.—CUI, W.—YU, S.—HAN, H.—HU, B.—LI, Y.: A Dual-Branch Dynamic Graph Convolution Based Adaptive TransFormer Feature Fusion Network for EEG Emotion Recognition. *IEEE Transactions on Affective Computing*, Vol. 13, 2022, No. 4, pp. 2218–2228, doi: 10.1109/TAFFC.2022.3199075.
- [18] ASADZADEH, S.—YOUSEFI REZAI, T.—BEHESHTI, S.—MESHGINI, S.: Accurate Emotion Recognition Using Bayesian Model Based EEG Sources as Dynamic Graph Convolutional Neural Network Nodes. *Scientific Reports*, Vol. 12, 2022, No. 1, Art.No. 10282, doi: 10.1038/s41598-022-14217-7.
- [19] YE, M.—CHEN, C. L. P.—ZHANG, T.: Hierarchical Dynamic Graph Convolutional Network with Interpretability for EEG-Based Emotion Recognition. *IEEE Transactions on Neural Networks and Learning Systems*, 2022, doi: 10.1109/TNNLS.2022.3225855.
- [20] TAVAKOLI, M.—BENUSSI, C.—LOPES, P. A.—OSORIO, L. B.—DE ALMEIDA, A. T.: Robust Hand Gesture Recognition with a Double Channel

- Surface EMG Wearable Armband and SVM Classifier. *Biomedical Signal Processing and Control*, Vol. 46, 2018, pp. 121–130, doi: 10.1016/j.bspc.2018.07.010.
- [21] CHEN, L.—FU, J.—WU, Y.—LI, H.—ZHENG, B.: Hand Gesture Recognition Using Compact CNN via Surface Electromyography Signals. *Sensors*, Vol. 20, 2020, No. 3, Art.No. 672, doi: 10.3390/s20030672.
- [22] CÔTÉ-ALLARD, U.—FALL, C. L.—DROUIN, A.—CAMPEAU-LECOURS, A.—GOSSELIN, C.—GLETTE, K.—LAVIOLETTE, F.—GOSSELIN, B.: Deep Learning for Electromyographic Hand Gesture Signal Classification Using Transfer Learning. *IEEE Transactions on Neural Systems and Rehabilitation Engineering*, Vol. 27, 2019, No. 4, pp. 760–771, doi: 10.1109/TNSRE.2019.2896269.
- [23] TORO-OSSABA, A.—JARAMILLO-TIGREROS, J.—TEJADA, J. C.—PEÑA, A.—LÓPEZ-GONZÁLEZ, A.—CASTANHO, R. A.: LSTM Recurrent Neural Network for Hand Gesture Recognition Using EMG Signals. *Applied Sciences*, Vol. 12, 2022, No. 19, Art.No. 9700, doi: 10.3390/app12199700.
- [24] LEEB, R.—SAGHA, H.—CHAVARRIAGA, R.—DEL R. MILLÁN, J.: A Hybrid Brain-Computer Interface Based on the Fusion of Electroencephalographic and Electromyographic Activities. *Journal of Neural Engineering*, Vol. 8, 2011, No. 2, Art. No. 025011, doi: 10.1088/1741-2560/8/2/025011.
- [25] LIN, K.—CINETTO, A.—WANG, Y.—CHEN, X.—GAO, S.—GAO, X.: An Online Hybrid BCI System Based on SSVEP and EMG. *Journal of Neural Engineering*, Vol. 13, 2016, No. 2, Art.No. 026020, doi: 10.1088/1741-2560/13/2/026020.
- [26] SARASOLA-SANZ, A.—IRASTORZA-LANDA, N.—LÓPEZ-LARRAZ, E.—BIBIÁN, C.—HELMHOLD, F.—BROETZ, D.—BIRBAUMER, N.—RAMOS-MURGUIALDAY, A.: A Hybrid Brain-Machine Interface Based on EEG and EMG Activity for the Motor Rehabilitation of Stroke Patients. 2017 International Conference on Rehabilitation Robotics (ICORR), 2017, pp. 895–900, doi: 10.1109/ICORR.2017.8009362.
- [27] TUN, N. N.—SANUKI, F.—IRAMINA, K.: Electroencephalogram-Electromyogram Functional Coupling and Delay Time Change Based on Motor Task Performance. *Sensors*, Vol. 21, 2021, No. 13, Art.No. 4380, doi: 10.3390/s21134380.
- [28] TUN, N. N.—SANUKI, F.—IRAMINA, K.: EEG-EMG Correlation Analysis with Linear and Nonlinear Coupling Methods Across Four Motor Tasks. 2021 43rd Annual International Conference of the IEEE Engineering in Medicine and Biology Society (EMBC), 2021, pp. 783–786, doi: 10.1109/EMBC46164.2021.9629969.
- [29] SOUNDIRARAJAN, M.—KREJCAR, O.—NAMAZI, H.: Evaluation of the Coupling Between the Brain and Facial Muscles Reactions to Moving Visual Stimuli. Fluctuation and Noise Letters, Vol. 20, 2021, No. 5, Art.No. 2150042, doi: 10.1142/S0219477521500425.
- [30] LUCIW, M. D.—JAROCKA, E.—EDIN, B. B.: Multi-Channel EEG Recordings During 3,936 Grasp and Lift Trials with Varying Weight and Friction. *Scientific Data*, Vol. 1, 2014, No. 1, Art.No. 140047, doi: 10.1038/sdata.2014.47.
- [31] AFSHANI, F.—SHALBAF, A.—SHALBAF, R.—SLEIGH, J.: Frontal-Temporal Functional Connectivity of EEG Signal by Standardized Permutation Mutual Information During Anesthesia. *Cognitive Neurodynamics*, Vol. 13, 2019, No. 6, pp. 531–540, doi:

- 10.1007/s11571-019-09553-w.
- [32] ANG, K. K.—CHIN, Z. Y.—ZHANG, H.—GUAN, C.: Filter Bank Common Spatial Pattern (FBCSP) in Brain-Computer Interface. 2008 IEEE International Joint Conference on Neural Networks (IEEE World Congress on Computational Intelligence), 2008, pp. 2390–2397, doi: 10.1109/IJCNN.2008.4634130.
- [33] YE, Y.—LIU, C.—ZEMITI, N.—YANG, C.: Optimal Feature Selection for EMG-Based Finger Force Estimation Using LightGBM Model. 2019 28th IEEE International Conference on Robot and Human Interactive Communication (RO-MAN), 2019, pp. 1–7, doi: 10.1109/RO-MAN46459.2019.8956453.



Lubo FU received his B.Sc. degree in information security from the Tongji University in 2021. Now, he is a graduate student in the Department of Computer Science and Technology, Tongji University. His research interests include machine learning and brain-computer interface.



Haoyang LI received his B.Sc. degree in software engineering from the Nantong University in 2020. Now, he is a graduate student in the Department of Computer Science and Technology, Tongji University. His research interests include machine learning and brain-computer interface.



Hongfei Ji is an Associate Professor with the Department of Computer Science and Technology, Tongji University, Shanghai, China. He received the Ph.D. degree in software engineering from the Tongji University, Shanghai, China, in 2015. His research interests include machine learning, pattern recognition, brain computer interface, and cognitive neuroscience.



Jie LI is an Associate Professor with the Department of Computer Science and Technology, Tongji University, Shanghai, China. She received the Ph.D. degree in computer science from the Shanghai Jiao Tong University, Shanghai, China, in 2010. Her research interests include machine learning, brain computer interface, brain like computation, and cognitive neuroscience.